Novel geometry for X-Ray diffraction mammary imaging: experimental validation on a breast phantom

Vera Feldman, Joachim Tabary, Caroline Paulus, Jean-Louis F Hazemann

Novel geometry for X-Ray diffraction mammary imaging: experimental validation on a breast phantom

Vera Feldman[a,b], Joachim Tabary[a,b], Caroline Paulus[a,b], and Jean-Louis Hazemann[c,d]

[a]Univ. Grenoble Alpes, F-38000 Grenoble, France
[b]CEA, LETI, MINATEC Campus, F-38054 Grenoble, France
[c]Univ.Grenoble Alpes, Inst NEEL, F-38042 Grenoble, France
[d]CNRS, Inst NEEL, F-38042 Grenoble, France

ABSTRACT

Mammography is the first tool in breast cancer diagnosis. Its contrast relies on the difference of X-Ray attenuation in healthy and diseased tissues, which is quite limited. This leads to frequent false-positive or inconclusive results and requires further testing. X-Ray Diffraction provides information about molecular structure and can differentiate between healthy and cancerous breast tissues. It can thus be used in synergy with existing imaging methods to provide complementary diagnosis-relevant insight.

We present a novel geometry of such an imaging system and its validation on a breast phantom composed of olive oil and beef muscle, imitating respectively the molecular structure of healthy and cancerous breast tissue. Our system combines energy-dispersive and angle-dispersive X-Ray diffraction by means of an energy-resolved CdZnTe detector and a multi-slit collimation in order to achieve depth-resolved imaging.

The position of the tube with beef muscle inside the oil was varied in this experiment. The obtained results are satisfactory regarding the estimated position of the tube which is very promising for future ex-vivo experiments on human breast tissue samples. Further investigations are carried out on dose reduction and reliable classification algorithms in order to prepare this method for clinical applications.

Keywords: Energy-dispersive X-Ray diffraction, Angle-dispersive X-Ray diffraction, X-Ray coherent scatter imaging, breast cancer diagnosis, tissue characterization, spectral imaging, CdZnTe detectors.

1. INTRODUCTION

Mammography is the most used tool in breast cancer screening and diagnosis. It is fast (less than 15 minutes for the whole procedure) and has excellent spatial resolution ($< 100\mu m$). Its source of contrast is the difference of X-Ray attenuation coefficients in different types of tissue: micro-calcifications and tumors appear brighter than healthy tissue. However, the difference of X-Ray attenuation in healthy and pathological breast tissue is rather small[1,2] and in some cases, may be insufficient for correct diagnosis.

X-Ray diffraction carries information about molecular structure and provides better contrast between healthy and cancerous breast tissue than attenuation-based techniques.[3] In 2017, Moss et al. demonstrated on breast tissue samples the correlation between the anatomopathological analysis, the golden standard in breast tissue diagnosis, and the data obtained by X-Ray diffraction.[4] It can thus be used as a complementary technique for breast cancer diagnosis or as a tool for surgical margin control in breast surgery.[5–9]

We present the results obtained with a novel geometry which combines energy- and angle-dispersive diffraction. We used a multi-slit secondary collimator for multi-angle selection and a CdZnTe energy-resolved pixelated detector. The diffracted spectra S_{diff} were measured for different pixels p and energies E on a breast phantom made of olive oil and a tube containing beef muscle, imitating healthy and cancerous breast tissue respectively. The measurements were reconstructed in order to assess the *form factors* $F(z, \chi)$ for different positions z and momentum transfers χ. These form factors reflect the molecular structure and show the difference between oil and muscle. The measurements were realized for different positions of the tube with muscle inside the phantom in order to estimate the system's accuracy regarding spatial resolution.

Medical Imaging 2019: Physics of Medical Imaging, edited by Taly Gilat Schmidt, Guang-Hong Chen, Hilde Bosmans,
Proc. of SPIE Vol. 10948, 109485O · © 2019 SPIE · CCC code: 1605-7422/19/$18 · doi: 10.1117/12.2511460

2. METHODS

The goal of our experiment is to estimate the form factor $F(z, \chi)$ of our phantom, z being the position along the beam axis, and χ the momentum transfer. Its definition is derived from Bragg's law :

$$\chi = \frac{E}{hc} sin(\theta/2) = \frac{1}{2d} \tag{1}$$

where E is the energy in keV, $hc = 1.24$ keV.nm is the product of the Planck's constant and of the value of light speed in vacuum, θ is the angle between incident and diffracted photon directions and d is the spacing between diffraction planes, used in crystallography. Unlike sharp diffraction peaks observed in crystallography, amorphous materials present a continuous distribution, called *form factor*, noted F hereafter.
In this section, we detail our acquisition setup and protocol, which yields diffraction spectra $S_{diff}(p, E)$ depending on detector pixels p and energy channels E. We briefly describe the model which links $S_{diff}(p, E)$ to $F(z, \chi)$ and the method we use estimate the form factor from diffraction spectra.

2.1 Acquisition setup

Our reconstruction process requires both transmission and diffraction measurements. They were acquired separately as the spatial configuration of our experimental bench does not allow simultaneous acquisition, but it will be considered in the future.

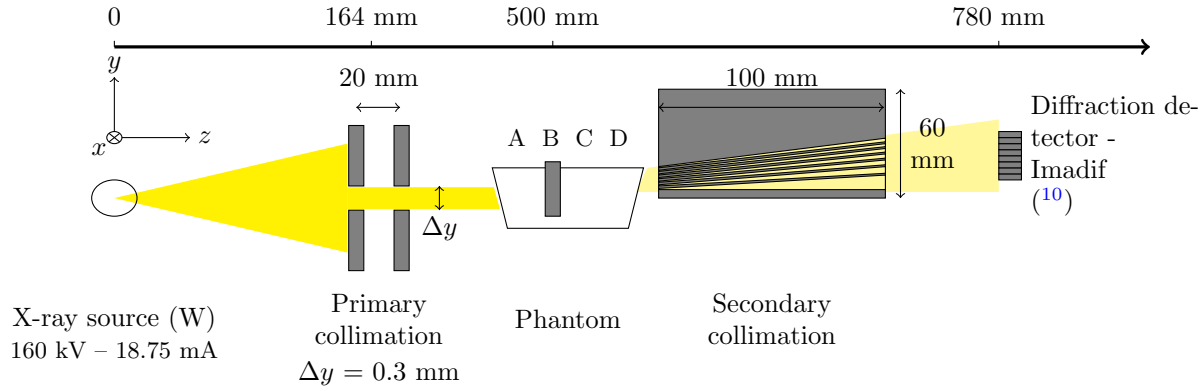

Figure 1: Experimental setup: system geometry (not to scale) for diffraction measurements. The letters above the phantom indicate possible positions of the tube inside the oil container.

2.1.1 Scatter acquisition

The experimental setup is shown schematically on figure 1. The tungsten-anode X-Ray tube was operated at 160 kV and 18.75 mA during 10 minutes. The beam was collimated with two slits into a 2 mm x 0.3 mm (x, y) pencil beam before reaching the sample.
The measurements were realized with our in-house energy-resolved detector Imadif.[10] It is composed of 24 rows and 8 columns (along y and x directions respectively) on a 660 mm^2 area. For the purposes of our experiment we used only row-wise pixels, the signal received column-wise was summed after angular correction.
Diffracted X-Rays were collimated using a multi-slit collimator designed by our team.[11] It is made of tungsten and has 7 slits with different angular opening aiming at different positions along z-axis, as can be seen on figure 2. The colored areas show, how the position of the object along z is translated into pixel position. Each color

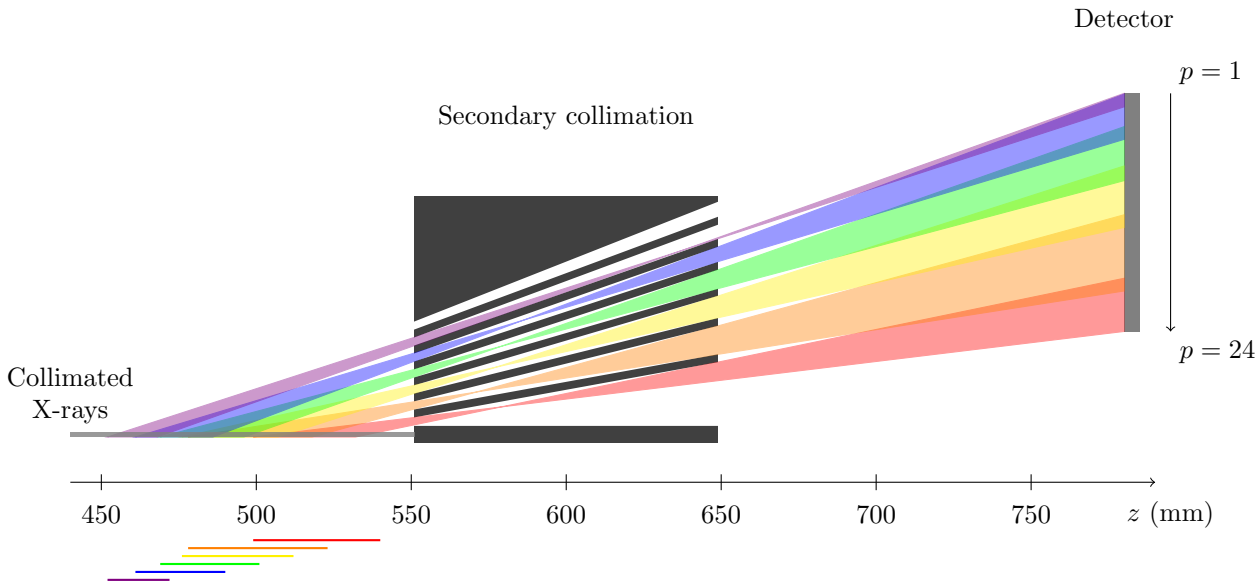

Figure 2: Scaled representation of the z positions seen by each slit. Below z-axis are shown the z-projections of the intersection between the field of view of each slit and the phantom volume illuminated by the X-Rays (gray area).

corresponds to one slit. z positions "seen" through different splits overlap slightly to cover the whole object area without gaps.
Calibration is required in order to learn the exact relation between z positions, pixels and diffraction angles. For this purpose we used a 3mm-thick aluminum plate. It was translated along z by 3 mm steps and diffraction spectra were acquired for each position. We used the aluminum diffraction peak corresponding to $\chi = 2.14$ nm^{-1}: for each z position of the calibration plate, we note the pixels, that "see" the aluminum plate at this position z, and corresponding energies. From this, we infer a matrix $M(p, z, \theta)$ representing the ratio between the number of photons seen by the pixel p coming from a position z at a diffraction angle θ, and the total number of detected photons. The 2-dimensional projections of this matrix are shown on the figure 3 : the subfigure (a) shows the relative diffraction intensity by pixel and z position and the subfigure (b) shows the diffraction angle depending on pixels and z positions.
These maps show that all the detector pixels are used to image a zone along the z axis between 480 and 540 mm. The zone between 500 and 540 mm will yield most photons, as this area corresponds to the first slit (lowest on the figure 2), which has the biggest opening. Each pixel "sees" a different zone, even though slight multiplexing is present. However, the diffraction angle varies rapidly between pixels, so we can expect good spatial resolution after reconstruction.

2.1.2 Transmission acquisition

The geometry used was exactly the same, except for the secondary collimation, which was removed, and a MultiX ME-100$^{\text{TM}}$ energy-resolved detector was used instead of the Imadif detector. The X-Ray tube was operated at 160 kV and 1 mA. The transmission acquisition is used to compute the attenuation of the sample, which is used in the reconstruction process to build the forward matrix described in the section 2.4.

2.2 Phantom

The phantom is represented schematically in (z, y) plane on figure 1 and a more detailed top view is shown figure 6. It is made of a thin plastic container filled with olive oil. A plate with cutout holes has been placed on top

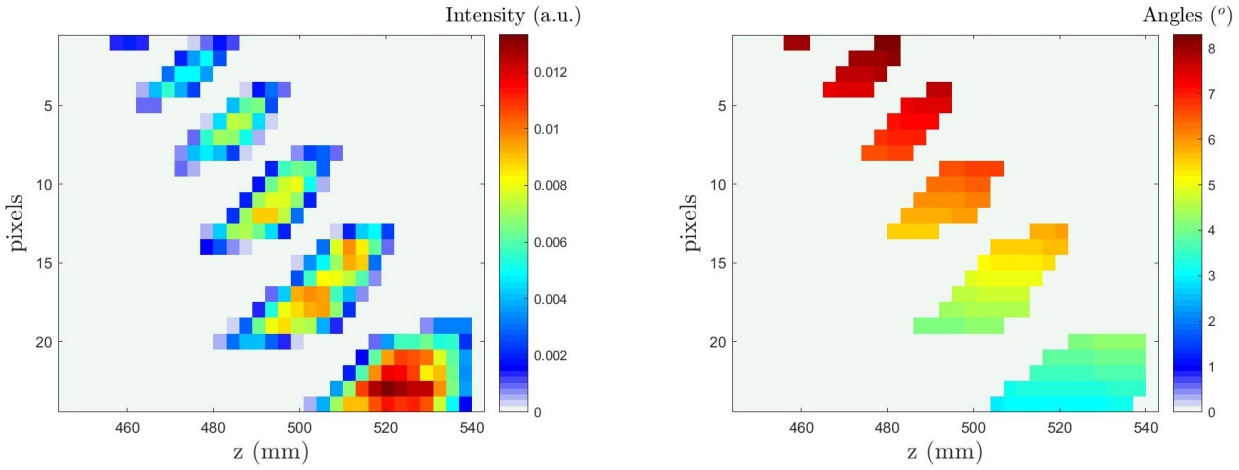

(a) (b)

Figure 3: Field of view obtained by calibration : diffraction intensity in a. u. (a) and diffraction angle in degrees (b) per z position and per pixel p

to hold one plastic tube containing beef muscle tissue at a chosen position along the beam direction. This way, oil occupies all the field of view along z, except one spot where the tube is placed. These positions are noted with letters going from "A" (closest to the source) to "D" (closest to the detector). On the figure 1 the tube is represented in the position "B". The figure 6 shows z-coordinates of each hole. During the acquisitions only one of the holes is occupied by the tube and oil occupies all the other z-positions.
Separation between the centers of consecutive holes is 15 mm. Tube's inner diameter measures 8 mm and its position along x axis is centered on the X-Ray beam.
Normalized reference form factors for adipose, well-differentiated cancer[12] and beef muscle[13] are shown on figure 4. Olive oil has been chosen because its form factor should be close to adipose tissue and present a peak at $\chi = 1.1$ nm^{-1} as does healthy breast tissue.[3] Beef muscle form factor has a fibrous peak[3] ($\chi = 1.6$ nm^{-1}) and imitates cancerous breast tissue's form factor.

2.3 Experimental protocol

The oil container remained at the same position through all the experiment so that the hole "B" was centered in $z = 500$ mm. 4 diffraction acquisitions were realized for different locations of the tube with beef muscle inside the oil container. An acquisition of olive oil without muscle has also been performed for reference. All diffraction acquisitions lasted 10 minutes.

2.4 Data analysis

The relation between form factor $F(z, \chi)$ and measured diffracted spectrum $S_{diff}(p, E)$ is modeled as follows:

$$S_{diff}(p, E) = R(p, E, z, \chi) \cdot F(z, \chi) \tag{2}$$

where p is the pixel number, E the detected energy, z the position along the beam axis and *chi* the momentum transfer. The forward matrix $R(p, E, z, \chi)$ models our whole experimental setup. It converts the form factor expressed in z, χ space into a diffracted spectrum, which is measured in p, E space. This matrix regroups the geometry, described by the matrix $M(p, z, \theta)$, the detector response matrix and the incident X-Ray spectrum attenuated by the sample. The geometry matrix $M(p, z, \theta)$ and the detector response matrix are both obtained by specific calibrations. The attenuated X-Ray beam is estimated using transmission acquisitions.
Inverting the model (2) is an ill-posed problem. In order to reconstruct F from S_{diff} we use a Maximum Likelihood Expectation Maximization (MLEM) algorithm.[14]

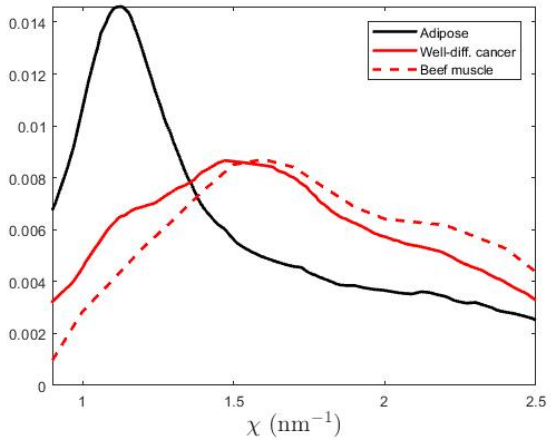

Figure 4: Normalized reference form factors of well-differentiated cancer (red line), beef muscle (red, dashed) and adipose (black)[12,13]

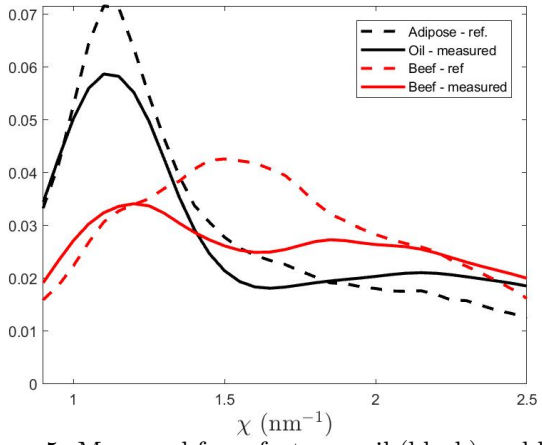

Figure 5: Measured form factors : oil (black) and beef muscle (red); Reference form factors: adipose (black, dashed) and beef muscle (red, dashed)[12,13]

3. RESULTS

Two-dimensional form factors $F(z, \chi)$ were reconstructed from $S_{diff}(p, E)$ and one-dimensional normalized form factors $F(\chi)$ have been obtained by averaging the 2D reconstructions on the respective locations of beef muscle and oil. They are presented on figure 5 along with reference form factors.[12,13] As expected oil has a distinct peak around 1.1 nm^{-1} and is very similar to the reference. For beef muscle measured and reference form factors are both rather flat, compared to oil and adipose, but not very similar, which is probably due to the oil signature smearing over the position of the tube. Still the difference between oil and beef muscle is clearly visible.
Figure 7 shows the reconstructed 2D form factors for tube positions from "A" to "D". For better visualization the form factors were corrected along z direction with the form factor of a homogeneous material (oil in this case) in order to remove some irregularities coming from the reconstruction process.
Adipose and beef muscle peak positions at, respectively, $\chi = 1.1$ nm^{-1} and $\chi = 1.6$ nm^{-1} are shown by vertical dashed lines (blue and red for adipose and beef respectively). Oil has a well-defined peak around this position. Black dashed lines indicate a 8mm-wide zone where the tube with beef muscle was positioned. We observe a zone with a flat form factor shifting depending on the tube position. This zone and the theoretical position of the tube are very similar which demonstrates the spatial accuracy of our system. Olive oil and beef muscle imitate respectively the form factors of healthy and cancerous breast tissue and these results are very encouraging for future acquisitions and diagnosis on human breast tissue.

4. CONCLUSION

We have presented a novel diffraction geometry, which combines angle- and energy-dispersive methods, and tested it on a 6cm-thick breast phantom. Reconstructed form factors $F(z, \chi)$ show accurate location of the 8mm-wide tube inside the oil container for each acquisition. This demonstrates spatial resolution within centimeter range. This is promising for future tests on human breast tissue samples.
A classification algorithm is going to be implemented in the near future for easier interpretation of the results. Short acquisition times and deposited dose are also two important criteria for clinical imaging. An experimental study is ongoing in order to determine the minimum dose and time, required to obtain insightful analysis.

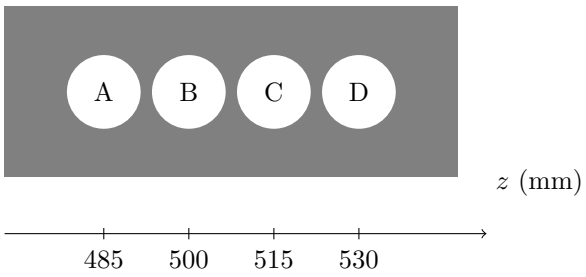

Figure 6: Top view ($x - z$ plane) of the phantom. In each separate acquisition the tube with beef muscle is located in one of the lettered holes and oil fills all the other positions.

REFERENCES

[1] Johns, P. C. and Yaffe, M. J., "X-ray characterisation of normal and neoplastic breast tissues," *Physics in Medicine and Biology* **32**(6), 675–695 (1987).

[2] Chen, R., Longo, R., Rigon, L., Zanconati, F., De Pellegrin, A., Arfelli, F., Dreossi, D., Menk, R.-H., Vallazza, E., Xiao, T., and Castelli, E., "Measurement of the linear attenuation coefficients of breast tissues by synchrotron radiation computed tomography," *Physics in Medicine and Biology* **55**(17) (2010).

[3] Kidane, G., Speller, R. D., Royle, G. J., and Hanby, A. M., "X-ray scatter signatures for normal and neoplastic breast tissues," *Physics in Medicine and Biology* **44**(7), 1791–1802 (1999).

[4] Moss, R. M., Amin, A. S., Crews, C., Purdie, C. A., Jordan, L. B., Iacoviello, F., Evans, A., Speller, R. D., and Vinnicombe, S. J., "Correlation of x-ray diffraction signatures of breast tissue and their histopathological classification," *Scientific Reports* **7**(1) (2017).

[5] Pani, S., "Applications of x-ray diffraction imaging to mammography," *Recent Patents on Medical Imaging* **2**(2), 111–119 (2012).

[6] Barbes, D., Tabary, J., Paulus, C., Hazemann, J.-L., and Verger, L., "Material-specific imaging system using energy-dispersive x-ray diffraction and spatially resolved cdznte detectors with potential application in breast imaging," *Nuclear Instruments and Methods in Physics Research A* **848**, 91–98 (2017).

[7] Marticke, F., Montémont, G., Paulus, C., Michel, O., Mars, J. I., and Verger, L., "Simulation study of an x-ray diffraction system for breast tumor detection," *Nuclear Instruments and Methods in Physics Research, Section A: Accelerators, Spectrometers, Detectors and Associated Equipment* **867**, 20–31 (2017).

[8] Feldman, V., Tabary, J., Paulus, C., Hazemann, J.-L., Filhol, O., Vilgrain, I., and Verger, L., "Ex-vivo mice mammary glands characterization using energy-dispersive x-ray diffraction and spacially resolved CdZnTe detectors," *Proc.SPIE* **10573** (2018).

[9] Spencer, J. R., Carter, J. E., Leung, C. K., McCall, S. J., Greenberg, J. A., and Kapadia, A. J., "Coded aperture coherent scatter spectral imaging for assessment of breast cancers: an ex-vivo demonstration," in [*Progress in Biomedical Optics and Imaging - Proceedings of SPIE*], (2017).

[10] Montémont, G., Kosciesza, D., Monnet, O., Stanchina, S., Schlomka, J. P., and Verger, L., "An autonomous czt module for x-ray diffraction imaging," in [*2013 IEEE Nuclear Science Symposium and Medical Imaging Conference (2013 NSS/MIC)*], (2013).

[11] Barbes, D., "Nouveaux systèmes d'imagerie médicale exploitant la diffraction x en dispersion d'énergie à l'aide de détecteurs spectrométriques CdZnTe," (2016).

[12] Pani, S., Cook, E. J., Horrocks, J. A., Jones, J. L., and Speller, R. D., "Characterization of breast tissue using energy-dispersive x-ray diffraction computed tomography," *Applied Radiation and Isotopes* **68**(10), 1980–1987 (2010).

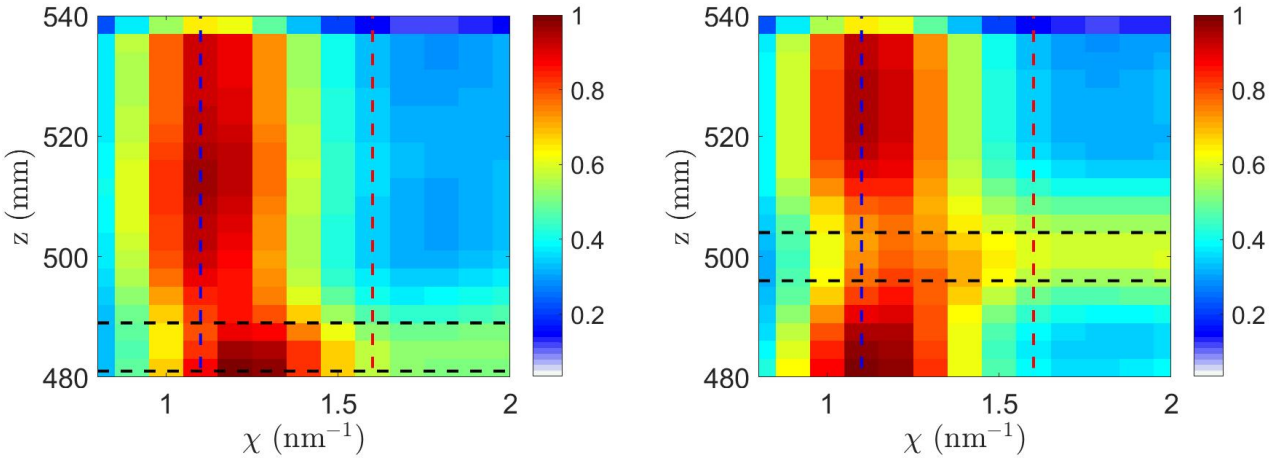

(a) Tube in "A"

(b) Tube in "B"

(c) Tube in "C"

(d) Tube in "D"

Figure 7: Reconstruction results for tube positions "A" (a) to "D" (d). Vertical dashed lines show the theoretical peak positions of adipose (blue) and beef muscle (red) positions. Horizontal dashed lines delimit the real position of the tube containing beef muscle tissue.

[13] Peplow, D. and Verghese, K., "Measured molecular coherent scattering form factors of animal tissues, plastics and human breast tissue," *Physics in Medicine and Biology* **43**(9), 2431 (1998).
[14] Shepp, L. A. and Vardi, Y., "Maximum likelihood reconstruction for emission tomography," *IEEE Transactions on Medical Imaging* **1**(2), 113–122 (1982).